The region of interest (ROI) of the specimen was determined by observing the two-dimensional amplitude image. Both the amplitude and phase in the ROI were measured for 10 MHz intervals between 100 to 210 MHz to obtain the quantitative values of acoustic properties. Thus, the frequency varying change of the amplitude and phase were obtained.

Figure 2 shows a schematic illustration of ultrasonic reflections at the tissue. The reflection (y_r) is assumed to be the sum of two components; one is the reflection from the surface of the tissue (y_s) and the other is the reflection from the interface between the tissue and glass (y_b). The interference of y_s and y_b are determined by the central frequency of the transmitted ultrasound.

The equation below shows the relationship between the frequency, amplitude and phase due to the interference between the reflection of the surface and bottom of the specimen. By fitting the obtained frequency varying curve with the calculated values, the thickness of the tissue in the ROI was obtained.

$$y_r = y_s + y_b$$
$$= R\,e^{-j\frac{2\pi f}{c}} + Ae^{-j2\pi f\,2d\left(\frac{1}{c_w}-\frac{1}{c}\right)}$$

(y_r: received signal, y_s: reflection from the surface of the specimen, y_b: reflection from the bottom of the specimen, $\boldsymbol{R}$: sound power coefficient of surface reflection, $\boldsymbol{f}$: frequency, $\boldsymbol{c}$: sound speed of the specimen, $\boldsymbol{d}$: thickness of the specimen, $\boldsymbol{A}$: slope of attenuation)

Figure 3 shows graphs of the relationship between the frequency and the amplitude or phase in a 5 μm thickness specimen.

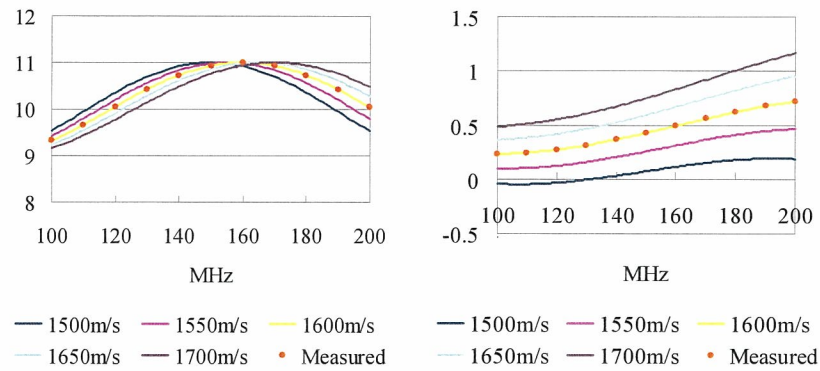

Figure 3. *Graphs showing frequency dependent characteristics of amplitude (left) and phase (right) in the frequency range between 100 and 200 MHz.*

Once the thickness of the specimen was determined, the attenuation and sound speed were calculated by the following equations.

$$A = \frac{10 \log(P / P_0)}{f d}$$

(A: slope of attenuation, P: sound power of reflection from the tissue, P_0: sound power of reflection from the glass, f: frequency, d: thickness)

$$c = \frac{1}{\frac{1}{c_w} - \frac{\theta}{2\pi f d}}$$

(f: frequency, d: thickness of the specimen, c: sound speed in the specimen, c_w: sound speed in the coupling medium, θ: phase shift)

Thus, quantitative values of slope of attenuation and of sound speed of each pixel can be obtained and this is the most important property of our scanning acoustic microscope system. The data of slope of attenuation and sound speed were converted into color signals and displayed on a color monitor as two-dimensional distribution patterns. Figure 4 shows the color bar scales of attenuation and sound speed.

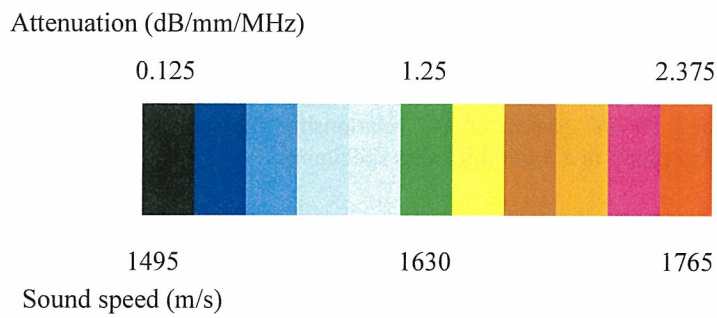

Figure 4. *Color scale of attenuation and sound speed used in the scanning acoustic microscope system at Tohoku University.*

For SAM examination, the tissue was frozen and sectioned at 10-μm by a cryostat and mounted on a slide glass. For optical imaging, the tissue was formalin-fixed, paraffin embedded and sectioned at 4-μm by a microtome. The specimen was stained with Elastica-Masson's trichrome and used for optical microscopy. The ROI for acoustic microscopy was determined by optical microscopic observations. The tissue components in normal and atherosclerotic arteries were classified as the following tissue components; normal intima, fibrosis, calcification, lipid, normal media and normal adventitia. The ROI was so determined that only a single tissue

component was included. Then, the mean values of attenuation and sound speed of each tissue component were averaged.

2.2 Sound speed acoustic microscopy

As described in the previous section, the acoustic microscopy developed in the 20th century has provided two acoustic parameters such as attenuation and sound speed and both parameters are useful for ultrasonic tissue characterization. However, it required several scans at the same portion with different frequencies for quantitative imaging. A new concept acoustic microscopy based on frequency domain analysis of a pulsed ultrasound instead of burst waves in the previous system has been developed since 2001. Figure 5 shows a block diagram of the system named sound speed microscopy. A single pulsed ultrasound with 5 ns pulse width was emitted and received by the same transducer above the specimen. The aperture diameter of the transducer was 1.2 mm and the focal length was 1.5 mm. The central frequency was 80 MHz and the pulse repetition rate was 10 kHz. Considering focal distance and the sectional area of the transducer, the diameter of focal spot was estimated as 20 μm at 80 MHz. Distilled water was used as the coupling medium between the transducer and the specimen. The reflections from the tissue surface and from the interface between tissue and glass were received by the transducer and were introduced into a digital oscilloscope (Tektronics TDS 5052, USA). The frequency range was 300 MHz and the sampling rate was 2.5 GS/s. Four times of pulse responses at the same point were averaged in the oscilloscope in order to reduce random noise.

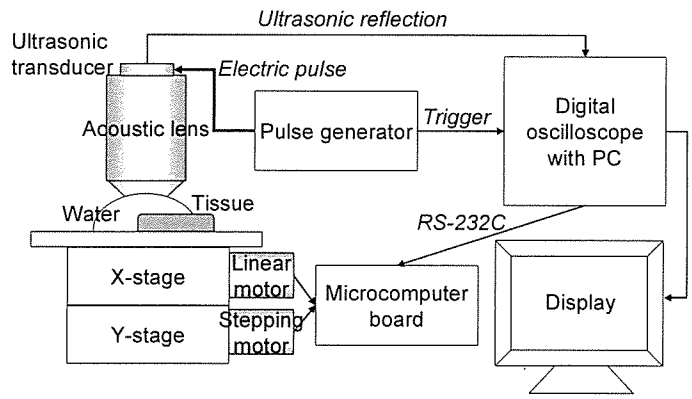

Figure 5. *Block diagram of sound speed scanning acoustic microscopy*

The transducer was mounted on an X-Y stage with a microcomputer board which was driven by the computer installed in the digital oscilloscope through RS-232C. X-scan was driven by a linear servo-motor and Y-scan was driven by a stepping motor. Finally, two-dimensional distributions of ultrasonic intensity, sound

speed and thickness of the specimen of 2.4 by 2.4 mm area were visualized with 300 by 300 pixels. Total scanning time was 121 sec.

Reflected waveforms are shown in Figure 6. The waveform at the glass surface without tissue is shown in (a). This signal was employed as a reference waveform. The decline of the glass surface was compensated by measuring three different points in the glass area surrounding the tissue. The waveform from the tissue area is shown in (b). Although the waveform contains two reflections at the surface and the interface of tissue and glass, two components cannot be separated in time domain analysis. Thus, the frequency domain analysis was performed by analyzing interference between two reflections. Intensity and phase spectra were calculated by Fourier-transforming the waveform. The spectra are normalized by the reference waveform. Figure 7 shows the frequency domain analysis of interfered waveform.

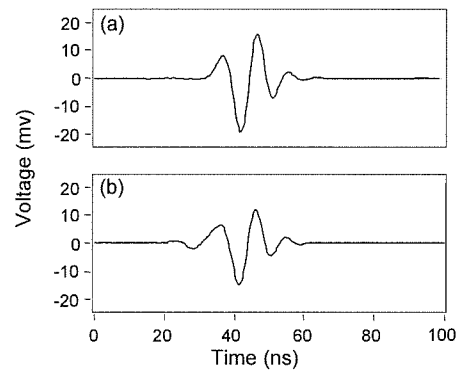

Figure 6. *Reflected waveforms (a) from the glass surface without tissue, and (b) from the tissue area.*

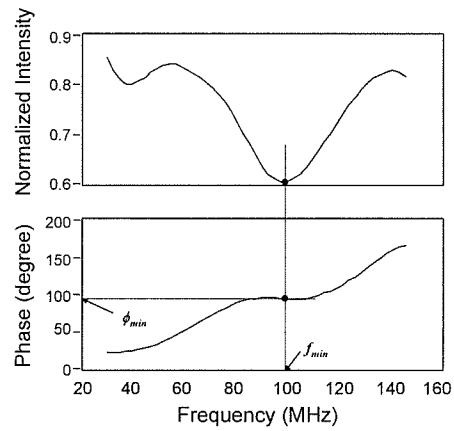

Figure 7. *Frequency domain analysis of interfered waveform.* f_{min}*: the minimum point in the intensity spectrum,* ϕ_{min}*: corresponding phase angle*

Assuming f_{min} as the minimum point in the intensity spectrum, and ϕ_{min} as the corresponding phase angle, the phase difference between the two reflections at the minimum point is (2n-1)π, giving

$$2\pi f_{min} \times \frac{2d}{c_o} = \phi_{min} + (2n-1)\pi$$

where d, c_0, and n are the tissue thickness, sound speed of the water, and a non-

$$2\pi f_{max} \times \frac{2d}{c_o} = \phi_{max} + 2n\pi$$

negative integer, respectively. Assuming f_{max} as the maximum point in the intensity spectrum, and ϕ_{max} as the corresponding phase angle, the phase difference at the maximum point is 2nπ, giving

The phase angle ϕ_{min} and ϕ_{max} can be expressed by

since ϕ_{min} or ϕ_{max} is the phase difference between the wave passed through the distance $2d$ with sound speed c and that passed through the corresponding distance

$$2\pi f_{min} \times 2d\left(\frac{1}{c_0} - \frac{1}{c}\right) = \phi_{min}$$

$$2\pi f_{max} \times 2d\left(\frac{1}{c_0} - \frac{1}{c}\right) = \phi_{max}$$

with sound speed c_0. By solving the above equations,

is obtained for the minimum point. For the maximum point,

$$d = \frac{c_0}{4\pi f_{min}}\{\phi_{min} + (2n-1)\pi\}$$

$$d = \frac{c_0}{4\pi f_{max}}(\phi_{max} + 2n\pi)$$

is obtained.

Sound speed at the each frequency is finally calculated as

$$c = \left(\frac{1}{c_0} - \frac{\phi_{min}}{4\pi f_{min} d}\right)$$

$$c = \left(\frac{1}{c_0} - \frac{\phi_{max}}{4\pi f_{max} d}\right)$$

2.3 Acoustic microscopy at 1.1 GHz

A scanning acoustic microscope (SAM2000; KSI, Herborn, Germany) was equipped for semi-quantitative ultrasonic measurements. In the present study, an acoustic lens with the optimal frequency range between 800 MHz and 1.3 GHz was used. The SAM frequency chosen in the experiments was 1.1 GHz because the image quality was best. Distilled water was used for the coupling medium between the transducer and the sample. The temperature of the transducer, coupling medium, sample and the glass substrate was maintained at 37 C° by a heating plate. The Rf output gain was fixed for all experiments. In the SAM system, an 80 dB difference of ultrasonic intensity corresponded to 256 gray scales (0-255). The reflection from the glass surface was set as level 255 (white). The average thickness of the specimen was determined by laser micrometer. Ultrasonic attenuation at each pixel was calculated from the number of the gray level and the thickness. All of the SAM images were stored in a personal computer for statistical analysis.

The optical and polarized images of atherosclerotic plaque were captured to make the same field taken by SAM. The images were analyzed using computer-assisted image analysis equipment (Leitz DMRBE light microscope; Leica Wetzlar, Germany, JVC KY-F55 color video camera; Victor Co.Ltd., Tokyo, Japan, Scion CG-7 RGB color frame grabber, and ScionImage; Scion Corporation, Frederick, MD, USA, and Photoshop; Adobe Systems Inc., Seattle, WA, USA). Although the picrosirius red staining was not a specific staining technique, the area with collagen was specifically visualized by polarized microscopy. The areas were differentiated according to the polarized color; longer wavelength (red or yellowish color) or shorter wavelength (green).

For the study at 800-1300 MHz, 11 normal human coronary arteries and 23 atherosclerotic aortae in Apo-E deficient mice were involved. The specimen was perfusion-fixed at 100 mmHg with phosphate-buffered 4% formaldehyde (PH 7.2) and immersed in the fixative overnight. The specimen was sectioned at 4-μm and embedded in paraffin. The paraffin was removed by a coconut oil and graded alcohol process for study. Unstained sections were used for the SAM investigations. After the SAM investigation, the sample was stained with Sirius red and covered by a cover glass. The same field observed by SAM is also observed by normal and polarized optical microscopy for comparing the tissue components.

To test the potential of acoustic microscopy, living cells were also visualized. Human renal artery smooth muscle cells were cultured on 35 mm diameter dishes with the Dulbecco's modified Eagle's medium and 10% heat-incubated bovine serum. The incubator was maintained at 37 °C and filled with 95% air and 5% CO2. Phosphate buffered saline was used for the coupling medium between SAM transducer and the cells. SAM images of a single cell were recorded by 3 minute intervals in order to detect the cellular motility. The difference between two consecutive frames was considered as the cellular motility. Calculated difference was colorized and overlayed on a SAM image.

3. Results

3. 1 Gastric cancer [SAI 91]

It is very important to detect cancer in an early stage and to distinguish malignant cells from benign tissues. With endoscopic ultrasonography, it is possible to observe submucosal invasions of cancerous tissue not detected by standard endoscopic biopsy. However, endoscopic ultrasonography cannot be used as yet for the classification of the gastric cancer. To determine the acoustic properties of each type of the gastric cancer tissue is thus important for understanding the clinical appearances of gastric cancer.

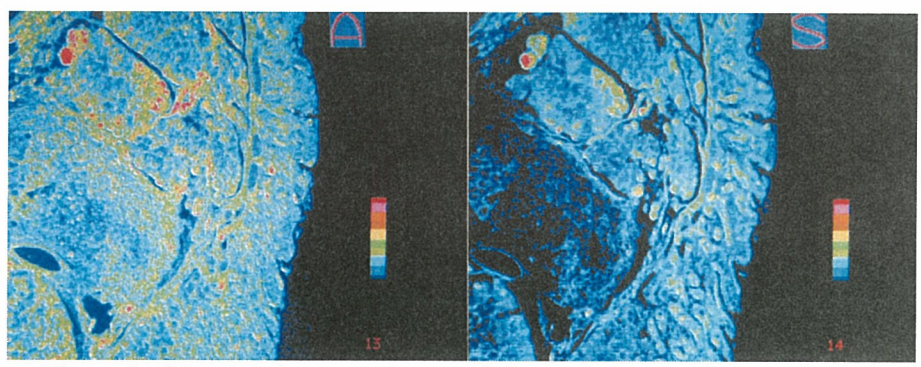

Figure 8. *Acoustic microscope images (left: attenuation, right: sound speed) of papillary adenocarcinoma.*

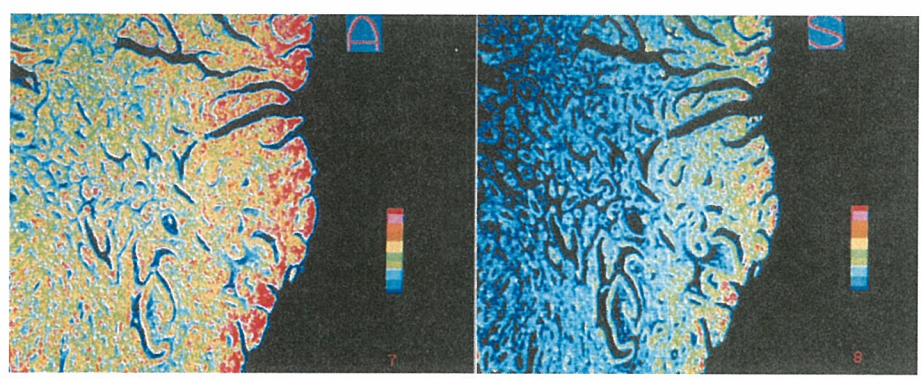

Figure 9. *Acoustic microscope images (left: attenuation, right: sound speed) of well-differentiated tubular adenocarcinoma.*

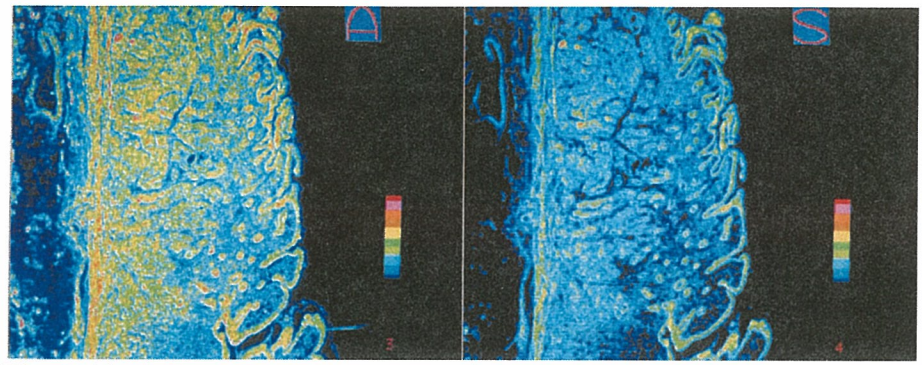

Figure 10. *Acoustic microscope images (left: attenuation, right: sound speed) of moderately-differentiated tubular adenocarcinoma.*

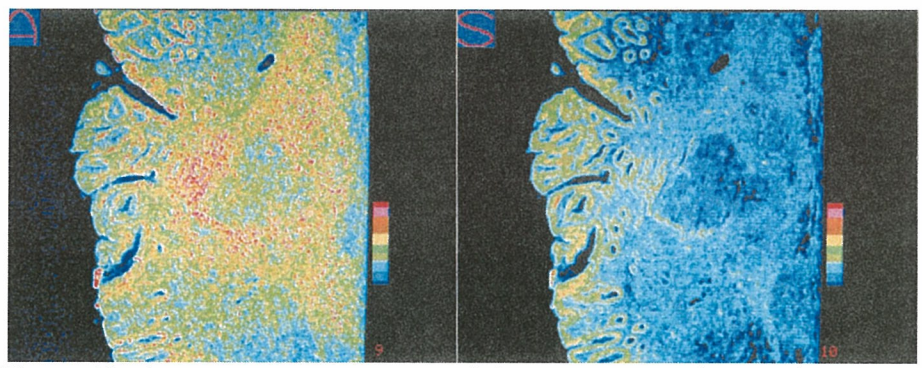

Figure 11. *Acoustic microscope images (left: attenuation, right: sound speed) of poorly-differentiated adenocarcinoma.*

The gastric cancer tissues were classified into five groups according to their pathological findings; papillary adenocarcinoma, well-differentiated tubular adenocarcinoma, moderately differentiated tubular adenocarcinoma, poorly differentiated adenocarcinoma, and signet-ring cell carcinoma.

Figure 8 is acoustic microscopic images of papillary adenocarcinoma. Papillary strucure of the cancer is clearly demonstrated in the image. Figure 9 is well-differentiated tubular adenocarcinoma, Figure 10 is moderately-differentiated tubular adenocarcinoma and Figure 11 is poorly differentiated adenocarcinoma, respectively.

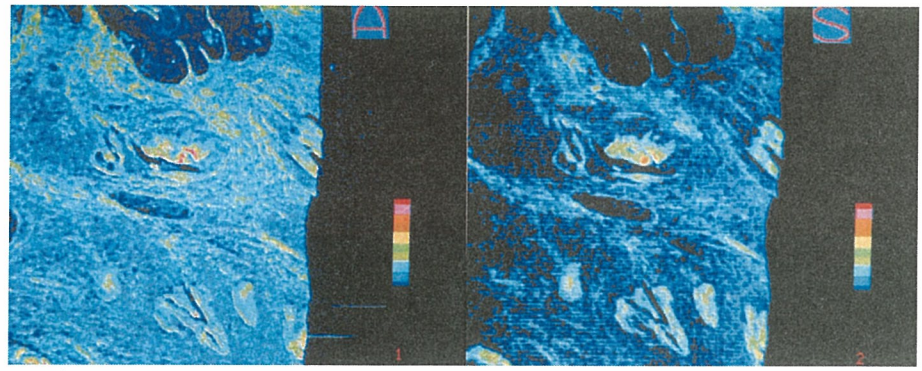

Figure 12. *Acoustic microscope images (left: attenuation, right: sound speed) of signet-ring cell carcinoma.*

Figure 12 is signet-ring cell carcinoma. For the signet-ring cell carcinoma specimens, the mean attenuation constant is 0.5 dB/mm/MHz and the sound speed is 1523 m/s, which are significantly lower than those of the normal mucosa and of the other types of gastric cancer tissues, except for poorly-differentiated adenocarcinoma.

Table 1 is the average and standard deviations of attenuation and sound speed.

Tissue type	Attenuation (dB/mm/MHz)	Sound speed (m/s)
Normal mucosa	1.0±0.5	1619±21
Well differentiated tubular adenocarcinoma	2.1±0.3	1667±17
Moderately differentiated tubular adenocarcinoma	1.4±0.1	1600± 5
Poorly differentiated adenocarcinoma	0.7±0.1	1557± 5
Papillary adenocarcinoma	1.1±0.1	1610±22
Signet-ring cell carcinoma	0.5±0.1	1523± 9

Table 1. *Average and standard deviations of acoustic properties of gastric cancer tissues.*

The values of the attenuation constant and the sound speed increased as the cellular differentiation proceeded through the three kinds of tubular adenocarcinoma. As the density of the biological soft tissues can be assumed to be nearly constant, increased sound speed can thus be interpreted to mean that tubular adenocarcinoma

tissues become acoustically stiffer as the differentiation of the tissue proceeds. Electron microscopy has shown that the number of desmosomes, which are considered to attach cell-to-cell, is significantly decreased in poorly differentiated adenocarcinoma. Well-differentiated tubular adenocarcinoma specimens exhibit nearly the same number of desmosomes as in normal mucosal tissue. This increasing trend was thus regarded as the result of tightening of the intercellular attachment.

Both the attenuation constant and the sound speed were significantly lower in the signet-ring cell carcinoma than in the adenocarcinoma. The intracellular component of the signet-ring cell carcinoma is the periodic acid, Schiff stain (PAS) positive substrate. The lower values of the attenuation and sound speed may be accounted for the intracellular chemical components of the tumor tissues.

These data of gastric cancer tumors clearly show that the SAM system can be used to classify the types of cancer tissues, as revealed by measurement of the acoustic parameters of the pathologies.

3. 2 Renal cell carcinoma [SAS 96]

Renal cell carcinoma is known to exhibit both low and high intensity echoes in clinical echography. Although the relationship between the echographic appearance and the histological appearance has been studied previously, the earlier studies did not reveal the nature of this relationship clearly. Thus, measurements of the acoustic properties at the microscopic level were considered to be important for understanding the clinically obtained echographic features.

Renal cell carcinoma is classified into two groups; clear cell subtype and granular (dark) cell subtype.

Figure 13 is the acoustic image of the clear cell subtype of renal cell carcinoma and the hemorrhage. Figure 14 is the acoustic image of the granular cell subtype.

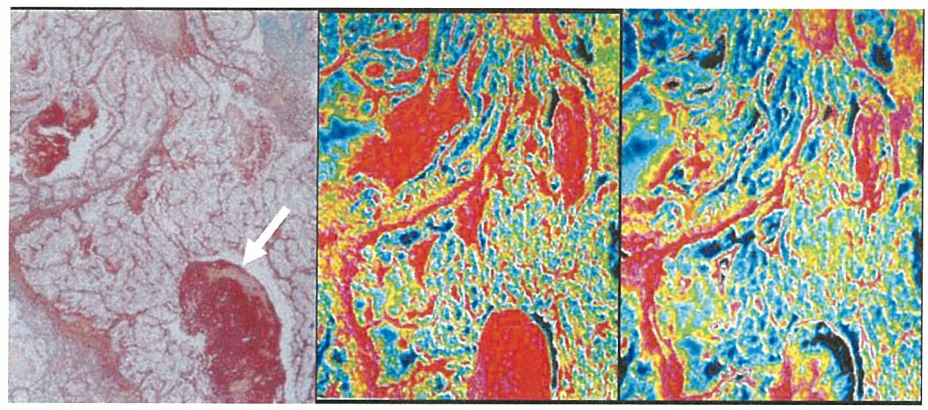

Figure 13. *Optical (left), attenuation (center) and sound speed (right) images of clear cell subtype of renal cell carcinoma. The arrow indicates hemorrhage.*

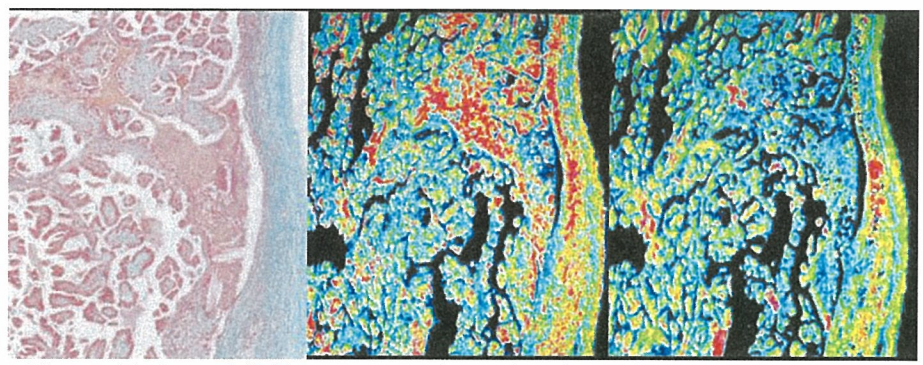

Figure 14. *Optical (left), attenuation (center) and sound speed (right) images of granular cell subtype of renal cell carcinoma.*

Table 2 shows the results of the measurement. The values of attenuation constant and sound speed are 1.15 dB/mm/MHz and 1624 m/s, respectively, for normal renal cortex. Both parameters have significantly lower values for clear cell and granular cell subtypes than those of normal cortex. No significant difference is seen between these two subtypes of renal cell carcinoma.

Both the attenuation constant and the sound speed show significantly higher values for hemorrhages and fibrotic tissues.

Tissue type	Attenuation (dB/mm/MHz)	Sound speed (m/s)
Normal cortex	1.2±0.2	1624±34
Normal medulla	1.1±0.2	1582±12
Clear cell subtype	0.4±0.1	1530±13
Granular cell subtype	0.5±0.2	1534±12

Table 2. *Average and standard deviations of acoustic properties of renal cell carcinoma tissues.*

The interface echo separating a pair of media is explained in terms of the magnitude difference of the two specific acoustic impedances. The difference of the acoustic impedance between clear cell and hemorrhage is very large, thus, a strong echo may be produced at the interface between the two types of tissue elements. However, the ideal reflection is usually discussed with the understanding that the fluid-like media are infinite and plane. The size of the hemorrhage in Figure 9 is about 500μm, and it is not clear how this size influences the reflection.

3. 3 Myocardial infarction[10]

Ultrasonic tissue characterization of myocardium has become very important because the needs of evaluating local cardiac function has been increasing. In the present study, acoustic properties of the tissue elements in myocardial infarction and dilated cardiomyopathy were measured and the elastic bulk modulus of the normal and pathological myocardium was assessed from the acoustic parameters.

Four kinds of tissue elements; normal myocardium, degenerated myocardium, granulation and fibrosis, were observed in the specimens.

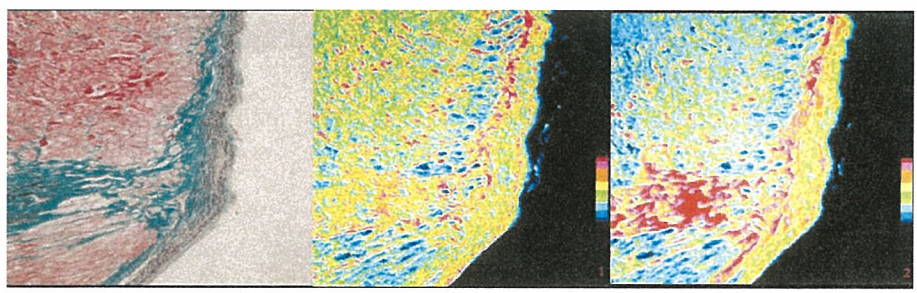

Figure 15. *Optical (left), attenuation (center) and sound speed (right) images of acute myocardial infarction.*

Figure 15 is the acoustic image of the myocardial infarction tissue. Fibrotic lesion represents high attenuation in this image. Table 3 is the results of the measurement.

Tissue type	Attenuation (dB/mm/MHz)	Sound speed (m/s)
Normal myocardium	0.9±0.1	1620±8
Degenerated myocardium	0.7±0.1	1572±11
Granulation	0.9±0.5	1590±33
Fibrosis	1.8±0.1	1690±9

Table 3. *Average and standard deviations of acoustic properties of acute myocardial infarction tissues.*

The sound speeds were 1620 m/s in the normal myocardium, 1572 m/s in the degenerated myocardium, 1690 m/s in the fibrosis, respectively. Density of each tissue element was measured by the graded $CuSO_4$ solution method, and the specific acoustic impedance was calculated by the sound speed and the density of each tissue element. The values were $1.75x10^6$ Ns/m^3 in the normal myocardium, $1.69x10^6$ Ns/m^3 in the degenerated myocardium, and $1.85x10^6$ Ns/m^3 in the fibrosis, respectively. On the assumption that the interface between two kinds of tissue elements is infinite and plane, the dB level of the relative reflected sound power can be calculated. The level at the inter face between degenerated myocardium and fibrosis is the greatest value among those considered in this study. The clinical echocardiography literature showed that the strong echoes were observed at the area of the scar in myocardial infarction. The origin of the strong echoes may be proposed by the present study.

As the biological tissues are modeled as fluid, the values of bulk modulus also can be calculated from the values of sound speed and density. The value of bulk modulus was $2.84x10^9$ N/m^2 in the normal myocardium, $2.65x10^9$ N/m^2 in the degenerated myocardium, $3.12x10^9$ N/m^2 in the fibrosis, respectively. Here it is seen that the elasticity of fibrotic tissue increases 10% and that of degenerated myocardium decreases 6% in comparison with normal myocardium. One of the roles of collagen fibers in acute myocardial infarction is to prevent the expansion of the infarction, and the frequency of left ventricular rupture has been reported higher in the group which exibits no remarkable increment of the scar in myocardium.

The elasticity of the fibrosis was considered to be adapted to the pathophysiology of myocardial infarction. The fibrosis in myocardial infarction is known to prevent the infarct expansion and the cardiac rupture.

3. 4 Heart transplantation [SAI 05]

A mouse received a heart transplant with a heterotopic abdominal model. The mouse was not given anti-immune drugs. The mouse was killed at 7 days after surgery. Histological specimens were prepared as to make a cross-section of the heart, and were sliced at 10-μm thickness for scanning acoustic microscopy and 4-μm for Elastica-Masson staining for optical microscopy. The specimen was ranked at AR grade 3 according to the following scale of increasing levels of allograft rejection (AR): AR grade 0 (normal), AR grade 1 (lymphocyte infiltration), AR grade 2 (focal necrosis), AR grade 3 (diffuse necrosis), AR grade 4 (presence of hemorrhages) as proposed in Journal of Heart and Lung transplantation.

The specimen was first scanned by the conventional SAM comparing with the optical microscope image of neighboring section. Then the same specimen was scanned again with sound speed acoustic microscopy so as to visualize the same view. These two kinds of images were largely compared and frequency-dependent characteristics of amplitude and phase of a region of interest were also compared.

Figure 16 shows (a) optical microscopic image, (b) attenuation image of conventional SAM, (c) sound speed image of conventional SAM, (d) intensity image of sound speed SAM, and (e) sound speed image of sound speed SAM, of a rat cardiac allograft model. Fig. 16 (a) shows that left part (inner part) is necrotic tissues with hyaline degeneration and right part (outer part) is normal myocardium. In Fig. 16 (b), the attenuation was 0.8 dB/mm/MHz in the necrotic tissue 1.2 dB/mm/MHz in the normal myocardium. In Fig.16 (c), the sound speed was 1580 m/s in the necrotic tissue and 1610 m/s in the normal myocardium. Intensity image was generated with two-dimensional distribution of a peak signal amplitude. Then the meaning of the image was different from the attenuation image of conventional SAM. In Fig. 16 (e), the sound speed was 1580 m/s in the necrotic tissue and 1610 m/s in the normal myocardium.

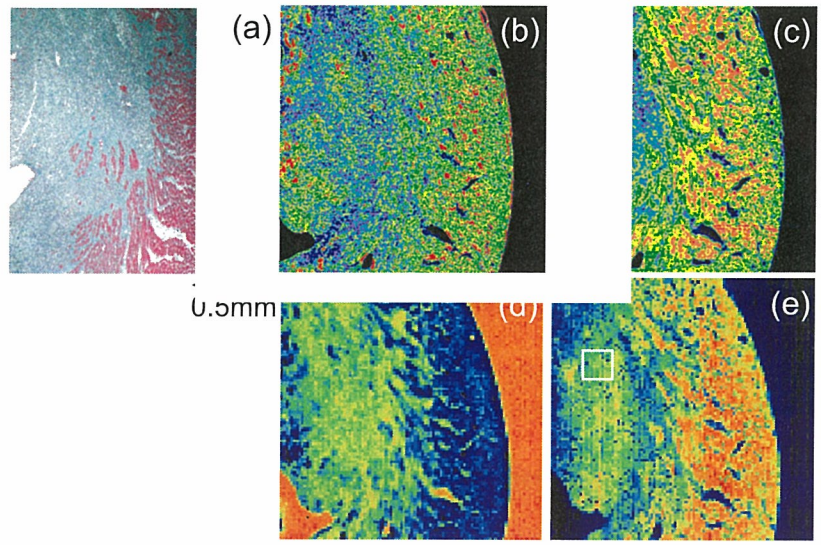

Figure 16. *(a) optical microscopic image, (b) attenuation image of conventional SAM, (c) sound speed image of conventional SAM, (d) intensity image of sound speed SAM, and (e) sound speed image of sound speed SAM, of a rat cardiac allograft model. ROIs are shown in Figure 16 (c) and 16 (e).*

3. 5 Atherosclerosis [SAI 98] [SAI 01]

Ultrasonic tissue characterization of atherosclerosis is important for two major reasons, the first, the acoustic parameters represent the physical properties of the atherosclerosis, and the second, the data provide important information of understanding the clinical appearance of intravascular ultrasound. The acoustic properties of the three layers in the normal and the atherosclerotic coronary arteries were measured.

Figure 17 shows the optical (a), attenuation (b) and sound speed (c) images of atherosclerotic human coronary artery visualized with the 100-200 MHz range acoustic microscope. Normal coronary artery is comprised of three layers; intima consisting of endothelium and thin collagen fiber, media consisting of smooth muscle and elastic fiber, and adventitia consisting of collagen fiber. In this image, the intima is thickened and a lipid core (L) underlying a thick "fibrous cap" (F) is observed in the intima. The lipid shows very low values of attenuation and sound speed compared with fibrosis. Figure 18 shows the optical (a), attenuation (b) and sound speed (c) images of atherosclerotic human coronary artery with coronary thrombosis. Newly organized thrombosis (T) shows higher values of attenuation and sound speed than those of the fibrosis (F).

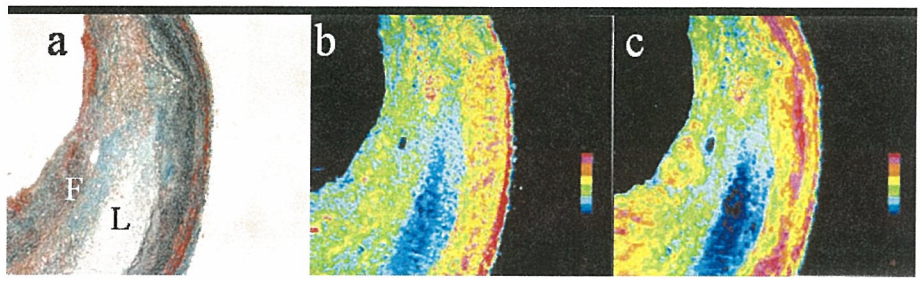

Figure 17. *Optical (left), attenuation (center) and sound speed (right) images of atherosclerotic coronary artery.*

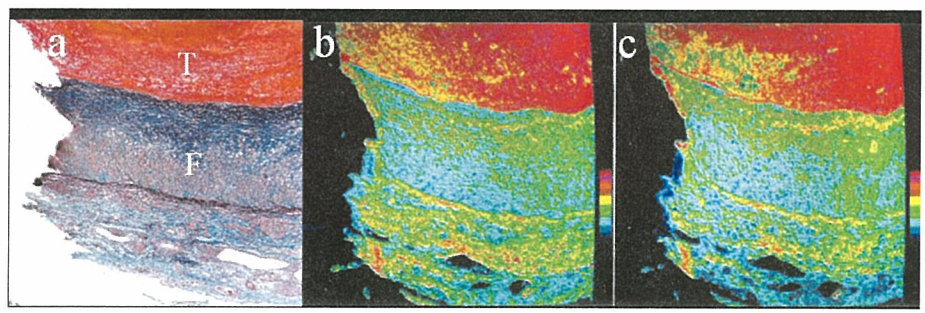

Figure 18. *Optical (left), attenuation (center) and sound speed (right) images of atherosclerotic coronary artery with coronary thrombosis.*

Figure 19 shows the optical (a), 200MHz (b) and 1.1GHz (c) acoustic microscopy images of normal human coronary artery. The image quality is better in 1.1GHz image. For example, each elastic fiber in the media can be observed in the 1.1GHz image while the media is almost homogeneous in the 200MHz image. However, the three-layered appearance of coronary artery is more obvious in the 200MHz image. The intima and adventitia show higher ultrasonic attenuation than that of media.

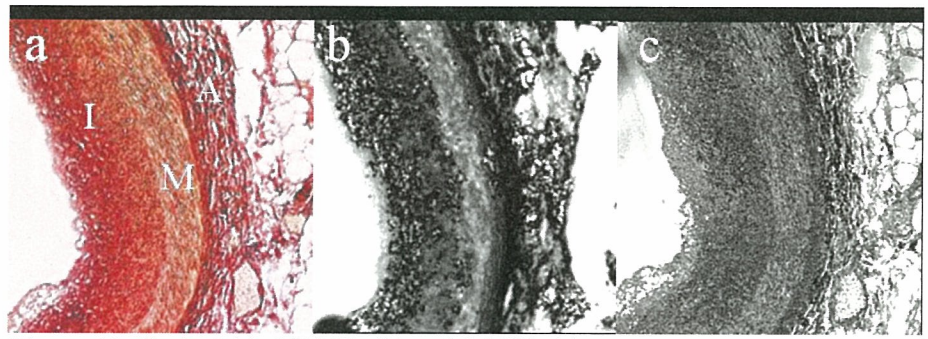

Figure 19. *Optical (a), 200MHz (b) and 1.1GHz (c) acoustic microscopy images of normal human coronary artery.*

Figure 20 shows the normal light (a), polarized light (b) and acoustic (c) microscopy images of a normal coronary artery. The ultrasonic frequency is 1.1 GHz. Endothelial cells aligning in a single layer and thin fibrosis comprise the intima. The smooth muscle cells and elastic fibers consisting of the media are shown by the acoustic image. Collagen fibers in the adventitia are highlighted by the polarized image. No pathological atherosclerotic lesions were found in this specimen.

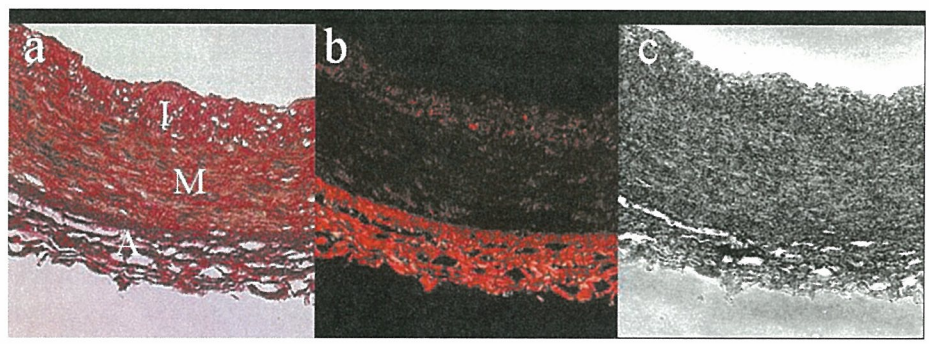

Figure 20. *Normal light (a), polarized light (b) and (c) acoustic microscopy images of normal human coronary artery.*

Figure 21 shows an atherosclerotic plaque found in a healthy young adult without a history of ischemic heart disease. The collagen network in the intima is shown. Although the lipid in the plaque was completely removed by alcohol dehydration, the remaining outer shape of the cholesterol crystal indicates that the cholesterol had existed in the spaces. The fibrosis in the plaque can be classified into

two categories by optical and acoustical findings; weak polarization and low ultrasonic attenuation, and strong polarization and high ultrasonic attenuation.

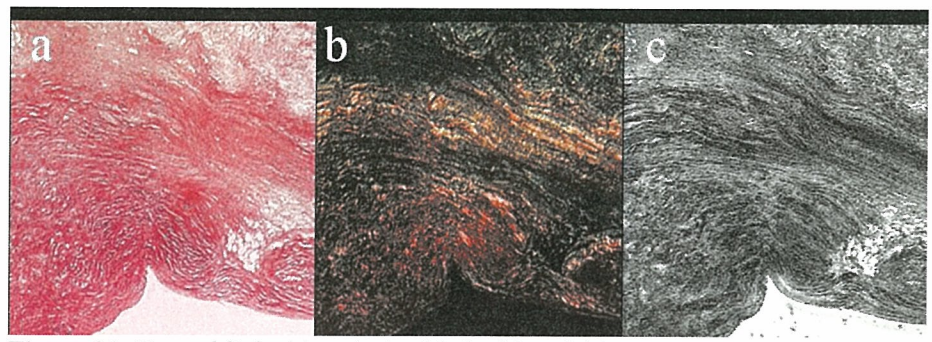

Figure 21. *Normal light (a), polarized light (b) and (c) acoustic microscopy images of atherosclerotic lesion found in a healthy young adult.*

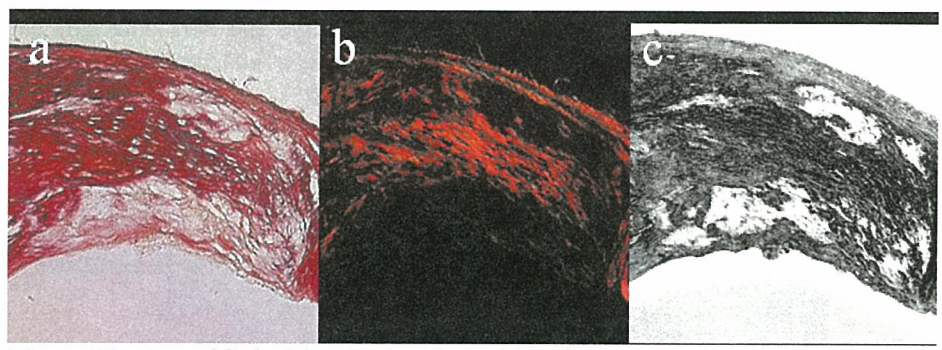

Figure 22. *Normal light (a), polarized light (b) and (c) acoustic microscopy images of thick fibrous cap in an Apo-E deficient mouse.*

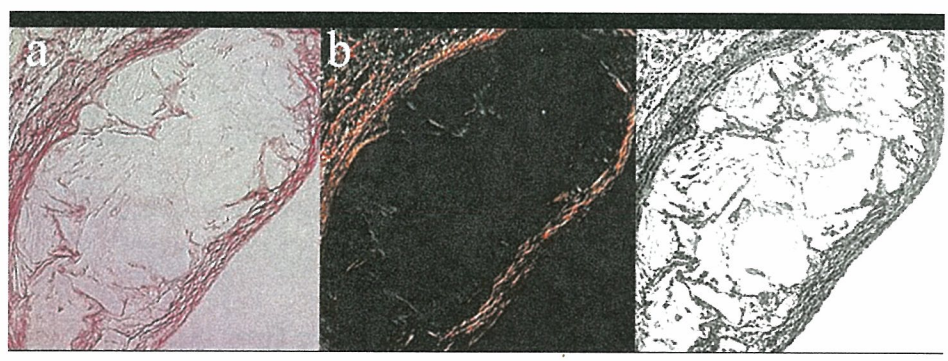

Figure 23. *Normal light (a), polarized light (b) and (c) acoustic microscopy images of thin fibrous cap in an Apo-E deficient mouse.*

Figure 22 shows a thick fibrous cap in an Apo-E deficient mouse. The fibrosis is strongly polarized in orange in the polarized image and shows high attenuation in SAM image. Figure 23 shows a thin fibrous cap in Apo-E deficient mouse. Thin fibrous cap overlying thick lipid pool is shown. In the lipid pool, some macrophages can be recognized by SAM image. The sparse collagen network in the lipid pool is polarized in apple green, which indicates type III collagen or thin collagen fibrils in polarized microscopy.

Tissue type	Attenuation ($x10^3$ dB/mm@1.1GHz)
Collagen (Type I)	17.2±2.6
Collagen (Type III)	6.6±2.1
Smooth muscle	4.7±1.9
Elastic fiber	15.5±2.4
Adventitia	16.1±2.1

Table 4. *Acoustic properties of tissue components of atherosclerosis in Apo-E deficient mice.*

Table 4 shows the results of the study on Apo-E deficient mice. Type I collagen characterized by orange polarized color in polarized microscopy showed high attenuation in acoustic microscopy. In contrast, type III collagen characterized apple green, showed low ultrasonic attenuation by acoustic microscopy.

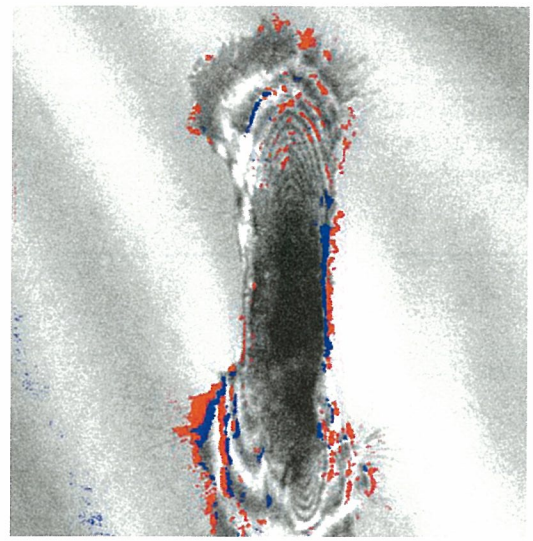

Figure 24. *SAM image of a human renal artery smooth muscle cell.*

Figure 23 shows a SAM image of a human renal artery smooth muscle cell. The cellular motility was colorized. Striations observed in the cell are produced by the interference between the surface and the bottom (interface between the cell and the plastic plate) of the cell. The interference can be considered as the difference of thickness. Blue indicates the difference between the previous and the present frames, while red indicates the difference between the present and the next frame.

4. Conclusions

The acoustic properties of biological tissues were obtained with two sets of scanning acoustic microscope system. Both systems were able to visualize high quality microscopy images suitable for histopathological examinations. The data suggest that the measurement of acoustic properties at the microscopic level is useful to characterize the types of cancer. The differentiation of cancer was also correlated with acoustic and mechanical properties of the cell type.

For cardiovascular tissues, micro-acoustic properties provided important information on biomechanical properties. Biomechanics of these tissues are especially important for assessing pathophysiology because the tissues are always receiving stresses such as blood pressure or blood flow. High frequency ultrasound can distinguish type III collagen from type I collagen fiber in atherosclerotic plaque